Propulsion and Power Research 2022;11(3):337–352

http://ppr.buaa.edu.cn/

Propulsion and Power Research

www.sciencedirect.com

ORIGINAL ARTICLE

Nacelle intake flow separation reduction at cruise condition using active flow control

Vinayak Ramachandran Nambiar*, **Vassilios Pachidis**

Centre for Propulsion Engineering, Cranfield University, Bedford, MK43 0AL, UK

Received 4 November 2021; accepted 22 July 2022
Available online 22 September 2022

KEYWORDS

Ultra high bypass ratio turbofan engine;
NASA Common Research Model;
Reynolds-averaged Navier-Stokes (RANS);
Computational fluid dynamics (CFD);
ANSYS Fluent;
Intake flow separation;
Active flow control;
Lip blowing

Abstract Turbofan engine intakes are designed to provide separation-free flow at the fan face over a wide range of operating conditions. But at some off-design conditions, like at high flight speeds and high angles of attack (AoA), the aero engine intake may encounter flow separation. This boundary layer separation inside the nacelle inlet of an aircraft engine can lead to a large number of undesirable outcomes like reduction in fan efficiency, engine stall and high levels of stress on the fan blades. Active flow control is a promising solution to reduce inlet boundary layer separation and the associated fan-face flow distortion at such off-design conditions. By blowing pressurized air into the intake near the separation point, the boundary layer is energized and separation can be controlled. This study investigates the applicability of lip blowing, an active flow control technique, to control intake separation and flow distortion at the fan-face. First, intake separation was triggered in a 3D CFD model based on the NASA Common Research Model (CRM) using high AoA cases at cruise condition (Mach number 0.85, Mass flow capture ratio ~0.7) and the features of separated flow were analyzed. Thereafter, active flow control was introduce to the intake in the form of two types of lip blowing, direct and pitched blowing. The efficacy of lip blowing at achieving separation control in an ultra high bypass ratio turbofan engine intake has been established through this study. The present paper also examines the significance of blowing parameters like the type of blowing, blowing pressure ratio, and blowing slot dimension, at different angles of attack to identify the critical control parameters. Our research successfully establishes proof of concept by demonstrating the

*Corresponding author.
E-mail address: vinayaknmbr@outlook.com (Vinayak Ramachandran Nambiar).
Peer review under responsibility of Propulsion and Power Research

Production and Hosting by Elsevier on behalf of KeAi

https://doi.org/10.1016/j.jppr.2022.07.005

feasibility of using lip blowing for separation control in aero-intakes, via numerical modelling. Furthermore, this study also provides crucial insights regarding the important variables to be considered for future experimental studies, and also for detailed studies covering a wider range of operating and blowing conditions.

Nomenclature

A	area (unit: m^2)
D	drag (unit: N)
D^*	modified drag (unit: N)
p	static pressure (unit: Pa)
P	total pressure (unit: Pa)
C_p	total pressure co-efficient
C_D	drag co-efficient
C_{D^*}	modified drag co-efficient
ρ	density (unit: kg/m^2)
Φ	stream force (unit: N)
τ	skin shear stress (unit: N)
m	mass flow rate (unit: kg/s)
q	dynamic head (unit: Pa)
v	flow velocity (unit: m/s)
M	flight Mach number

Subscripts

pre	pre entry to engine
nac	nacelle
post	post exit from engine
out	nacelle outer
in	nacelle inner
th	nacelle throat
ss	stagnation
ref	reference
ff	fan face
∞	free stream/ambient conditions
pre	pre entry to engine

1. Introduction

Aircraft nacelle are designed to provide smooth flow of air to the engine inlet with minimum aerodynamic losses (Luidens et al. [1]). They are equipped with a sufficiently long, thick and curved lip to provide a surface along which the flow can accelerate gradually without separation and total pressure loss, especially at off-design conditions. But in cruise conditions, where the aircraft spends the majority of its time and fuel, the thickness and length of the lip contribute towards nacelle drag, and therefore towards fuel consumption [1]. This has been a significant problem in high bypass turbofan engines, and is further exacerbated in modern ultra-high bypass engines which have a fan diameter of over 3 m. Applying boundary layer flow control techniques in the intake could be a viable alternative to using the geometry of the nacelle to control flow separation, enabling the use of thinner, streamlined, shorter and more aggressive intakes (Peters et al. [2]). The benefits from this include fuel savings for the aircraft, reduced emissions and a larger AoA envelope. Moreover, the reduced weight due to the reduction in nacelle size could improve airframe integration and reduce both the isolated nacelle drag, and the associated interference drag (Lord et al. [3]).

Flow separation, when it occurs inside the intake of an aero engine nacelle, creates a region of recirculation and low pressure within the intake, resulting in very high flow distortions at the engine fan face. This non-uniform pressure distribution at the fan face shifts the fan working line and transiently raises it, which may in turn lead to engine surge, sudden and erratic thrust variations and could produce stresses capable of jeopardising the structural integrity of the fan blades. Freeman and Rowe [4] determined a common pattern which followed intake separation, whereby the fan operating line rises along with the intake distortion. If the distortion and the associated pressure drop are severe enough the fan would drop to rotating stall; then as the flow rate falls, the intake recovers from separation but the fan stays locked in stall due to hysteresis. They also found that for the fan to recover from stall once the intake has recovered from separation, the fan would have to be operated at a very low working line.

To optimise the performance of the engine, separation in the intake needs to be controlled. Boundary layer control involves “any mechanism or process through which the boundary layer of a fluid flow is caused to behave differently than it normally would were the flow developing naturally along a smooth straight surface.” (Flatt [5]). Such methods have long been employed to achieve a wide range of outcomes like reduction in drag, increased lift, improved flow mixing, flow-related noise suppression, etc. [6]. Although there are no universally accepted definitions, flow control techniques are broadly classified as active and passive flow control, based on the energy expenditure of the system (MacMynowski and Williams [7], Gad-el-Hak [8,9]). Passive control devices, which require no external energy input to operate, include modifications to the aerofoil geometry like longitudinal grooves and riblets, ramps, domes, scoops, etc. (Lin et al. [10]). There are also the widely used vane vortex generators (VG’s); wedge shaped vanes affixed to the aerofoil surface, having thickness of the

order of the boundary layer and positioned at a small incidence to the flow. They all facilitate local mixing, and therefore energy exchange, between the boundary layer and free stream flow; making them simple, cheap and relatively efficient. As the name suggests the major disadvantages of such devices are their inability to provide dynamic and adaptive control, and also their impact on efficiency due to aerofoil drag at cruise conditions where they are not usually necessary (Schubauer et al. [11]).

Alternatively active flow control can be dynamic and adaptive based on the system operating conditions, but requires an external energy supply. Prandtl [12] carried out the earliest trials with the method of suction, using an adverse pressure gradient to remove the boundary layer. Suction is inefficient as it removes the fluid in the boundary layer, and also because the maximum adverse pressure gradient that can be achieved reduces with ambient pressure. Wallis [13] proposes the use of air jets blown into the fluid stream to improve mixing and momentum transfer within the boundary layer, by generating longitudinal stream-wise vortices, similar to passive VG's, for separation control. A study by Johnston and Nishi [14] of Air Vortex Generator Jets (AVGJ) using an array of such jets with varying position, pitch, skew and velocities of jets concluded that separation can be substantially reduced, or even eliminated, with the right control conditions. Erbslöh and Crowther [15] observed that for turbofan intake separation control, distortion reduce by 34% by using AVGJ's with 0.1% of the bleed mass flow. Kumar and Alvi [16,17] monitored the variation in the pressure coefficient along a ramp and achieved significant C_p recovery using an arrays of micro-jets (very small air jets with diameter = 400 μm). Though a promising method, the micro-jets are hard to simulate using commercial CFD software because of the extremely fine mesh required to capture the flow features of the micro-jets within a large turbofan intake. Synthetic Jets are another relatively new technique that uses the periodic motion of a diaphragm, piston, or acoustical device to synthesize a control jet within an orifice. The periodic motion creates the effect of alternative suction and expulsion of fluid from and into the boundary layer, effectively resulting in a zero net mass flux. This method is very efficient and requires very low power input if the acoustic excitation device is operated near resonance (Amitay [18], Amitay et al. [19]). McCormick [20] studied synthetic jets embedded in a wall adjoining the boundary layer and found that when tested in a diffuser, it could achieve nearly 45:1 return on the electrical power input. Inherent delicacy of components like diaphragms, which are easily damaged in the extreme conditions to which they may be subjected to on-board an aircraft, and the large size necessary of other mechanisms like pistons for the large mass flow of an aircraft make them unsuitable for use in civil large engines (Tesar et al. [21]).

Slot blowing is a type of injection control, similar to vortex jets, in which fluid is blown into the boundary layer to compensate for the energy loss due to skin friction. When Kühn et al. [22,23] carried out numerical investigation of slot blowing on the flaps of a high-lift wing-body geometry, using a RANS solver and different turbulence models, they observed that with steady slot blowing, only partial separation was present, as opposed to complete separation without blowing. Further investigations revealed that when the blown air is directed perpendicular to the free stream flow, it could trigger separation. Tangential blowing is a technique used to avoid this effect. Studies by Johns et al. [24] for NASA on a V/STOL tilt nacelle, with slot blowing at different blowing pressure ratios, angles of attack and forward velocities, revealed that tangential blowing tremendously improved intake performance. They concluded that with this method, improved pressure recovery, reduced flow distortions, significantly low blade stresses, and an increase of separation free angle of attack from 61° to 110° could be achieved.

As per the understanding of the authors, the application of active flow control in ultra-high bypass turbofan engines has not been studied previously. Therefore, as a novel strategy, this study examines the feasibility of lip blowing for separation control in aero-intakes, and attempt to establish a proof of concept for this method. To this end, intake flow separation was triggered in a scaled up 3D model of the NASA CRM model, using very high AoA cases at cruise conditions, with steady RANS simulation. Then lip blowing was applied to the intake, and its effects on flow features, and efficacy in reducing flow separation and the associated losses were determined.

The Environment Control Systems (ECS) in modern engines, which uses compressor bleed air for their functioning, are largely oversized to meet safety requirements. Integration with innovative ECS architectures, such as the cabin blower system, could provide the pressurized air supply required for lip blowing, without putting any extra load on the engine.

2. Drag accounting method and distortion descriptors

The thrust and drag book-keeping system used by the Cranfield University Propulsion Systems Installation and Integration team has been modified and used to extract the drag values from the simulation data. This method is derived from the method put forward by the North Atlantic Treaty Organization (NATO) AGARD Ministry Industry Drag Analysis Panel Study Group [25], whereby for an unducted nacelle, drag (D) can be defined as the sum of the pressure forces acting on the nacelle (Φ_{nac}), including forces due to the pre-entry (Φ_{pre}) and post-exit (Φ_{post}) stream tubes (Figure 1 and Eq. (1)). The pre-entry stream force (Φ_{pre}) can be expressed as the difference between the gauge stream forces at the section corresponding to the stagnation point (F_{ss}) and that at a section infinitely upstream of the nacelle (F_{∞}) (Eq. (2)).

In practice, the post exit stream force (Φ_{post}) has negligible effect on intake performance, so to reduce numerical

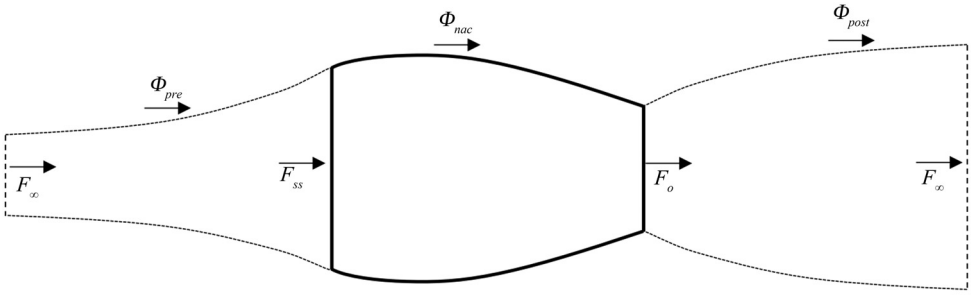

Figure 1 Force definition for an unducted nacelle.

complexity and simplify the cases, a 'Modified Drag' term (D^*) is used (Eq. (3)). For a ducted nacelle housing an engine, to calculate the pre-entry stream force (Φ_{pre}) we need to account for the stream forces acting on the fan-face section (F_{ss}), the stream forces at a section infinitely upstream of the nacelle (F_∞), and also the force exerted by the stream tube on the inner surface of the nacelle ($\Phi_{nac,in}$) which is equal in magnitude but acts opposite in direction to the gauge stream forces (Eq. (4)). Including the pressure force acting on the outer surface of the nacelle as a separate variable ($\Phi_{nac,out}$), the modified drag equation becomes Eq. (5). While running the CFD cases, we need to define the fan-face as a pressure outlet boundary, therefore, it is not ideal to retrieve stream force data from this boundary for accuracy. We adapt the drag extraction method to define a section named 'lip_end_plane' at the throat of the nacelle, using which gauge forces at that plane ($\Phi_{nac,th}$) can be extracted from CFD data. Note that when we move the reference plane upstream, only the stream tube forces acting on a smaller section of the nacelle from the stagnation point to the throat plane (F^*_{ss}), need to be accounted for while calculating the pre-entry stream force (Figure 2 and Eq. (6)). The modified drag used in this study is given by Eq. (7).

$$D = \Phi_{pre} + \Phi_{nac} + \Phi_{post} \tag{1}$$

$$\Phi_{pre} = F_{ss} - F_\infty \tag{2}$$

$$D = \Phi_{pre} + \Phi_{nac} \tag{3}$$

$$\Phi_{pre} = F_{ff} - F_\infty + \Phi_{nac,in} \tag{4}$$

$$D^* = F_{ff} - F_\infty + \Phi_{nac,in} + \Phi_{nac,out} \tag{5}$$

$$\Phi_{pre} = F^*_{ss} - F_\infty + \Phi_{nac,th} \tag{6}$$

$$D^* = F^*_{ss} - F_\infty + \Phi_{nac,th} + \Phi_{nac,out} \tag{7}$$

The value of F^*_{ss} can be obtained by integrating the axial forces on the cross-section of the throat. F_∞ is calculated using Eq. (8) from the engine mass flow rate (m_e) and flight speed (V_∞), which in turn is a function of flight Mach number and ambient temperature (Eq. (9)). Values of $\Phi_{nac,in}$ and $\Phi_{nac,th}$ can be determined directly from CFD data by integrating Eqs. (10) and (11) over the outer nacelle cowl till the trailing edge, and inside the nacelle till the throat. We also define parameters which can be used for benchmarking purposes, like the modified drag coefficient (C_{D^*}) which is the ratio of the modified drag to the product of the free stream dynamic head and the reference area (A_{ref}) of the body (Eq. (12)). The value of reference area for a CRM nacelle is defined as 383.68 m^2 by Vassberg et al. [26], halved to 191.84 m^2 as only half the area is used for the model.

$$F_\infty = m_e V_\infty \tag{8}$$

$$V_\infty = M\sqrt{\gamma R T_\infty} \tag{9}$$

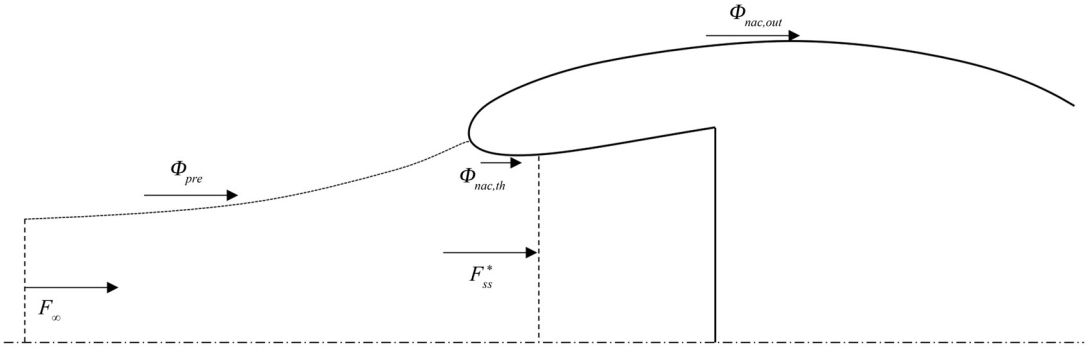

Figure 2 Adapted method for extracting modified drag from CFD data.

$$\Phi_{nac,out} = \int_{A_{nac,out}} [(p - p_\infty) + \tau_\omega \cot\theta] dA \tag{10}$$

$$\Phi_{nac,th} = \int_{A_{nac,th}} [(p - p_\infty) + \tau_\omega \cot\theta] dA \tag{11}$$

$$C_{D^*} = \frac{D^*}{\frac{1}{2}\rho_\infty V_\infty^2 A_{ref}} \tag{12}$$

To quantify the distortion encountered by the engine fan-face, two commonly used distortion descriptors are used in this study. $DC(\theta)$ descriptor is a widely used method introduced by Seddon and Goldsmith [27], in which the measurement face is divided into equal sectors having an internal angle θ. Then the $DC(\theta)$ value can be defined as the difference between the average total pressure on the face (P_{avg}) and the lowest value of average total pressure of any individual sector ($P_{\theta,min}$), non-dimensionalised by the flow dynamic head at that face (q) (Eq. (13)). θ can be any value depending on the requirements, therefore in this case 120° was selected so as to capture the entire region where the effect of separation would be present. The DC descriptors can be used both in CFD and in an experiment set-up using rakes, making them especially useful if the results need to be compared with experimental results. One more parameter, the total pressure coefficient $C_{p,ff}$ which is the ratio of the average total pressure at the engine face ($P_{avg,ff}$) to the total pressure of the free stream flow (P_∞) (Eq. (14)), is used to quantify distortion. It should be noted that the $C_{p,ff}$ value varies inversely with distortion since it is a measure of the pressure loss, whereas the $DC(\theta)$ increases with increase in distortion as it is a direct measure of the distortion.

$$DC(\theta) = \frac{P_{avg} - P_{\theta,min}}{q} \tag{13}$$

$$C_{p,ff} = \frac{P_{avg,ff}}{P_\infty} \tag{14}$$

3. Computational methodology and convergence strategy

Owing to the plethora of experiments which has been carried out (Levy et al. [28], Vassberg et al. [29], etc.), the NASA Common Research Model [30] is the ideal candidate for studies aimed at benchmarking CFD results. A 3D model is necessary to completely capture the flow features since the NASA CRM geometry is not symmetric about any axis, but the geometry is such that it is symmetric about a central plane. The grid was generated by adapting a verified mesh created by Stańkowski et al. [31,32] of a simple through flow nacelle. The mesh was suitably modified to include all the relevant features to recreate the effect of an engine on the nacelle. Two planes, named as the 'fan_face' and the 'engine_exit', were defined inside the nacelle to represent the engine, and another plane, named as the 'lip_end_plane', was added at the end of the nacelle lip to extract the nacelle drag (Figure 4(c)(d)).

A grid convergence study has been carried out with three levels of mesh density varying from coarse to fine to superfine, with 7.4, 11.4 and 15.6 million cells respectively, and using two mesh sets with different first cell wall $y+$ values (Table 1). Richardson Extrapolation (RE) has been used for the grid convergence study, and thereby verifying the accuracy of the model (Celik et al. [33], Roache [34], Slater [35]). An extrapolated value of drag coefficient of the nacelle, adjusted for spatial discretization errors was derived (Figure 3).

The grid convergence study showed good agreement with the results for the different meshes sets, with the extrapolated value of the modified drag coefficient obtained for both the mesh sets being equal to the fifth decimal point.

From Richardson Extrapolation (RE):

- For Mesh Set 1, $C_{D^*} = 0.00121$
- For Mesh Set 2, $C_{D^*} = 0.00121$

The data required for this analysis was taken from the results obtained by running the simulations for all the meshes with the typical cruise conditions for a civil large aircraft; 35000 ft altitude, at 0° AoA, and flight a flight Mach number of 0.85 as the boundary conditions. This boundary condition was also selected as it was the simplest

Table 1 Grid convergence study with 3 different mesh densities and 2 different first wall cell distance.

	Grid type	No. of nodes	$\dot{m}_{ff}$/(kg/s)	D^*/kN	C_D^*	Wall $y+$
Set 1	Coarse	7.4	340.59	2.53	0.00109	4.72
	Fine	11.5	339.97	2.71	0.00117	3.95
	Superfine	15.2	338.91	2.78	0.00120	3.27
Set 2	Coarse	7.4	340.78	2.44	0.00106	3.68
	Fine	11.5	340.14	2.62	0.00113	2.03
	Superfine	15.2	339.20	2.73	0.00118	1.32

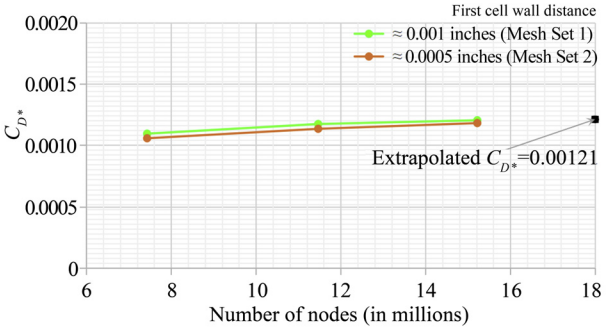

Figure 3 Richardson Extrapolation showing extrapolated value of drag co-efficient.

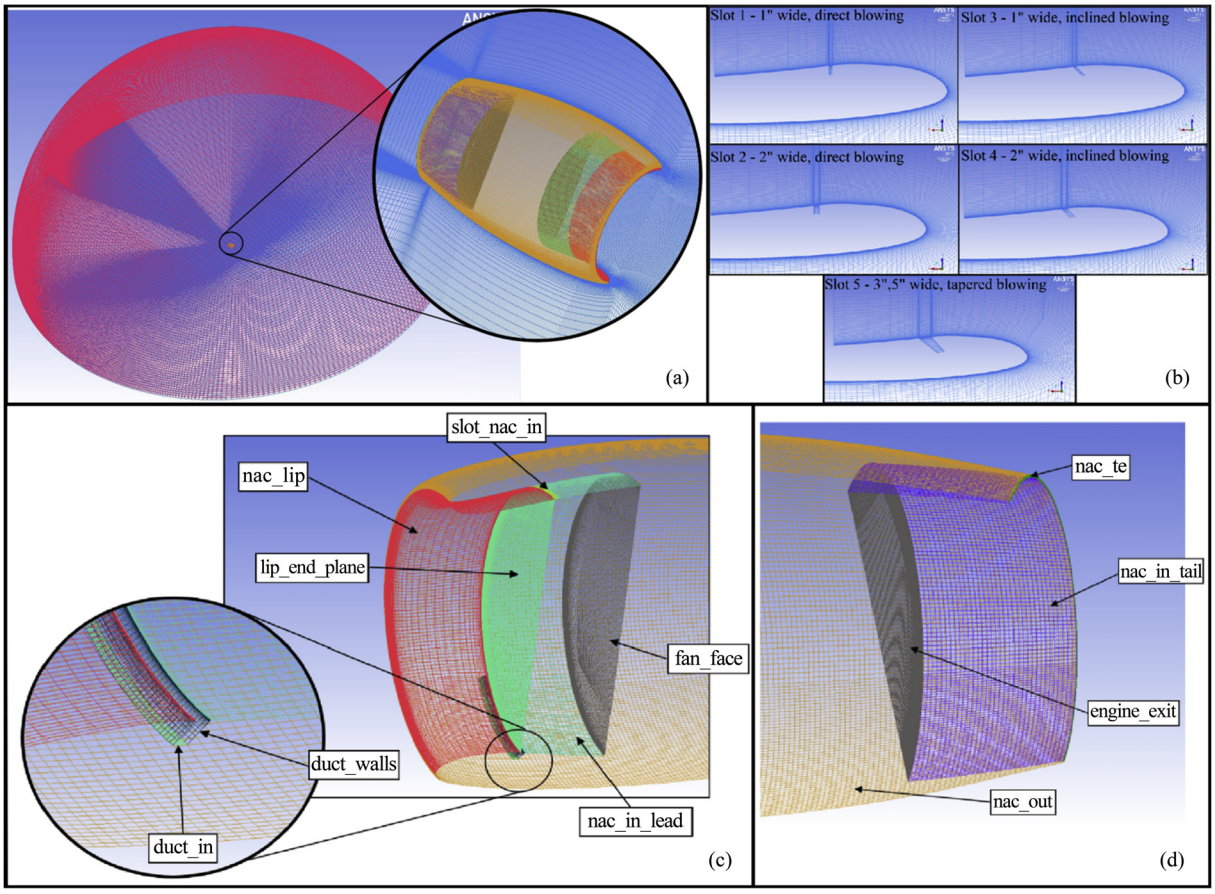

Figure 4 (a) The 'Final mesh' of the nacelle within the flow domain, (b) slot variants tested, (c) flow boundaries near the engine intake, (d) flow boundaries near the nozzle.

way to trigger separation from the perspective of a RANS CFD simulation using high AoA cases, while keeping the CRM geometry unchanged for validation purposes. The mass flow capture ratio (MFCR), another aerodynamic variable of significance, defined as the ratio of the area of the free stream stream-tube which enters the engine and the highlight area of the nacelle, was restricted to ∼0.7. The fine mesh with 11.5 million cells and a higher first cell wall distance was chosen as the 'Final mesh' to run all the remaining cases for AoA study and slot blowing study, serving as a good trade-off between accuracy and computation time.

It was not possible to directly validate the CFD model since there is no publicly available experimental test data for an isolated nacelle. Therefore, the development of the drag accounting technique and the mesh sensitivity analysis is dedicated to improving the credibility of the computational methodology. Additionally, the values of drag coefficient extracted was compared with the results from Stańkowski et al. [31,32], and showed good agreement. Furthermore, the experimental values obtained from tests conducted at the NASA Ames and US National Transonic Facilities and presented at the sixth AIAA CFD drag prediction workshop (Tinoco et al. [36], Rivers [37]) with a WBNP (Wing Body with Nacelle and Pylon) configuration were comparable with this study after accounting for interference drag effects.

To incorporate slot blowing into the intake, new sections and boundaries were defined, as shown in Figure 4(c). Blowing air would be supplied by applying a positive pressure gradient on the duct_in boundary. The slots were located immediately after the throat of the nacelle, i.e. where the intake diffuser began. Since the separation due to steeper AoA occurred at the bottom of the nacelle, all the slots were confined to the lower quarter of the nacelle and extended circumferentially for 45° from the plane of symmetry. Five different slot variations have been considered in this study, shown in Figure 4(b). The first slot, Slot 1 is one inch wide and oriented normal to the surface, providing direct blowing which is perpendicular to the free stream. Slot 3 is one inch wide again, but now inclined 45° to the nacelle surface and would provide pitched blowing at a 45° angle to the free stream. This pitched blowing has been done to reduce the possibility of blowing induced separation. Slot 2 and Slot 4 are 2 inches wide each, and Slot 2 is normal to the surface, while Slot 4 is pitched at 45°.

To improve the accuracy of the result, and create a better flow field approximation, a blowing duct was also modelled with each of the slots. The ducts for the direct slots (Slot 1

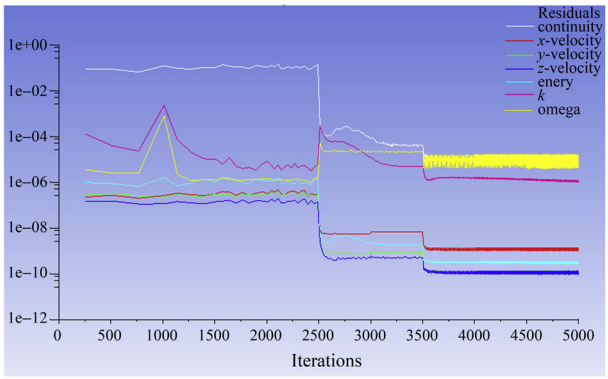

Figure 5 Residual plot showing convergence history.

and 2) were 3 inches long and the ducts for the pitched slots (Slot 1 and 2) were 4.2 inches long. The fifth and final slot, Slot 5, consisted of a tapered, diverging duct for diffused pitched blowing. It was 5 inches wide at the nacelle surface and 3 inches wide at the inlet of the blowing duct, and was made 8.2 inches long to capture the diffusion process in the duct. All five mesh grids consisted of 12 million elements. The control parameter used to assess the performance of blowing is the blowing pressure ratio (PR), defined as the ratio of total pressure applied at the duct inlet to the free stream total (P_∞) pressure. The boundary condition for the duct inlet was total pressure inlet. FLUENT defines total pressure as gauge pressure, therefore atmospheric pressure (p_∞) was subtracted from the free stream total pressure for the blowing duct inlet gauge total pressure boundary condition (Eq. (15)).

$$P_{gauge,\ duct\ inlet} = (PR \times P_\infty) - p_\infty \tag{15}$$

After the cases were set up with the boundary conditions mentioned earlier, initialization was carried out with the ANSYS FLUENT Full Multigrid (FMG) initialization to give an initial solution with suitable accuracy in a relatively short time. This was done to generate a more realistic flow field during initialization, than that which would have been obtained from the Standard or Hybrid initialization options in FLUENT. For a large and complex domain, like the one in consideration in this study, this would help accelerate convergence. To account for the flow turbulence effects accurately, the two equation k-ω SST RANS model is used (as in Kühn et al. [22,23] and Stańkowski et al. [31,32]) throughout the simulation. The pressure based solver was found to converge faster than the density based solver and was also more stable, therefore it was used in the beginning to take advantage of this feature and speed up convergence. Since the flow fields in the cases under this study consist of regions of transonic flow, the solver was switched to the density based solver with implicit formulation and the Roe-FDS (flux-difference splitting) before final convergence, to improve the accuracy of the results. All the discretization terms (pressure, density, momentum, turbulent kinetic energy, specific dissipation rate and energy) were set to the second order and the Green-Gauss Node Based scheme was used to compute the gradient. The convergence was monitored until a threshold of 10^{-5} was achieved for the continuity, k and ω residuals, and all the other residuals were comfortably below an order of magnitude 10^{-8} (Figure 5).

4. Results and discussion

4.1. Angle of attack study

The angle of attack study was carried out on the final mesh by increasing the AoA in steps of 5°, up-to a maximum AoA of 20°, and the modified drag and fan-face distortion were calculated through post processing of the simulation data. Since the accuracy of the model was validated at the typical conditions of cruise, this was retained as the boundary condition for the AoA and slot blowing studies as well. The variation of modified drag extracted with the angle of attack from each of the cases is plotted in Figure 6. The CRM nacelle is designed to be installed at an incidence angle of 5°, and therefore provides the best aerodynamic performance in this position. As a result the baseline case with 0° incidence is an off-design condition, resulting in the initial reduction of the C_{D^*} measured between 0° and 5°. As the AoA is increased to 10°, the stagnation point on the upper lip moves inward and the air stream moving along the cowl undergoes stronger acceleration as it navigates around the lip. This can be seen as the high Mach regions near the leading edge on the outer surface of the nacelle in Figure 7. The maximum flow Mach number has increased from 1.29 to 1.54 between 5° and 10° respectively. This stronger acceleration reduces the static pressure along the cowl leading edge, creating a cowl suction effect in the forward direction and resulting in the reduction of drag, which can be observed at 10° incidence.

4.2. Flow separation and intake distortion

Considering the separation feature inside the intake, the first instance of reversed flow at the fan_face was observed at 15°, which had a comparatively small and localised separation near the fan_face. Even though the separation in this case is very small, a visible reduction in fan_face total pressure recovery can be seen; as a region of low pressure at

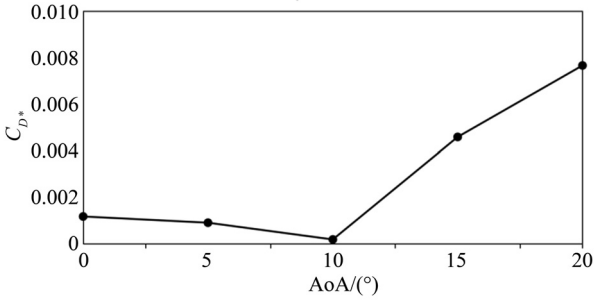

Figure 6 C_D* variation with angle of attack.

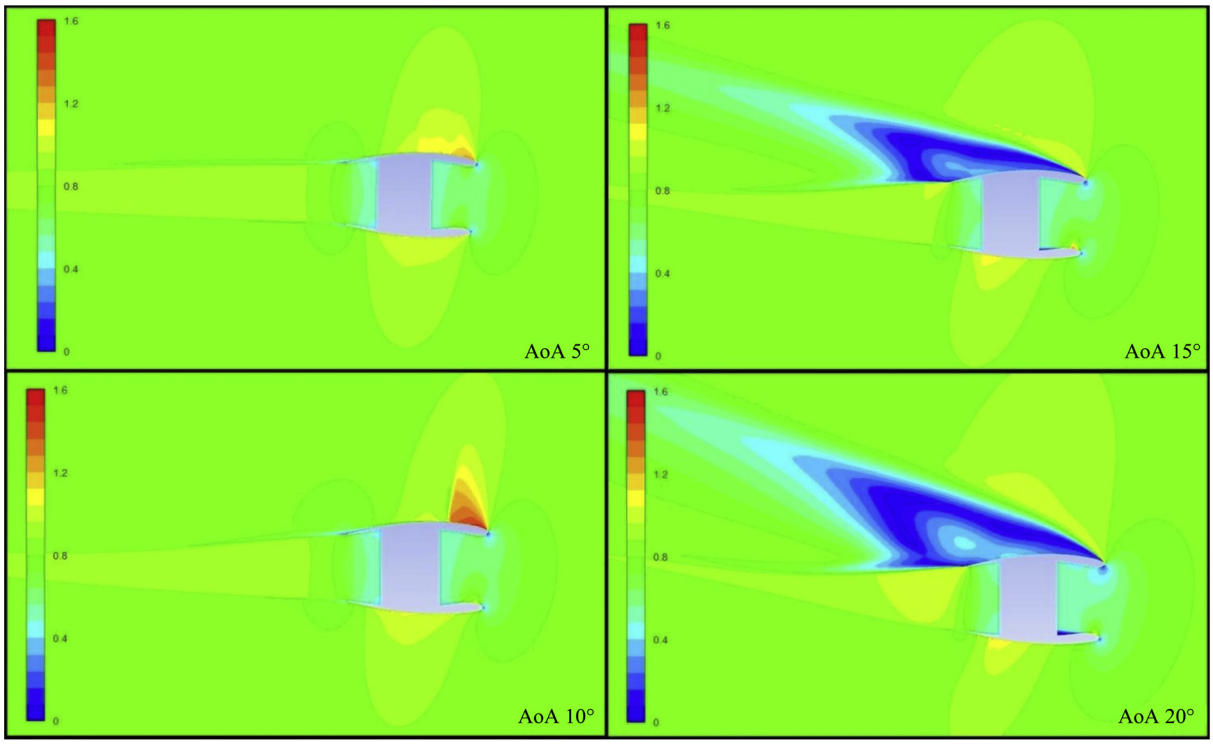

Figure 7 Mach number contours around the nacelle on the plane of symmetry.

the bottom of the fan_face, close to the plane of symmetry in Figure 8(a). This clearly shows that the separation first occurs along the base of the inner surface of the nacelle, causing this dip in total pressure. The separation is accompanied by a rise in the *DC*(120) distortion descriptor and a reduction in the total pressure co-efficient (Figure 8(b)(c)). On increasing the AoA to 20°, the low pressure region on the fan_face has grows considerably, indicating that there is strong separation and recirculation, and also that the separation point has moved further upstream from the fan-face than when it was at 15°. Velocity contours taken from the fan-face and the nacelle interior was used to identify and study the reversed flow regions of separation in the intake (detailed analysis in Section 4.3.3. and Figure 13).

On closer examination a curious feature emerges from the results which is present only in the 20° AoA case. In the 20° incidence case in Figure 8(a), there is a small region with a noticeable rise of total pressure and axial velocity near the central plane, close to the bottom of the fan face, where the pressure suddenly peaks. It was concluded that this non-uniformity could only be due to the presence of separation induced vortices inside the intake. Such phenomenon has been noted previously in studies which deal with S-Duct intakes with vane VG flow control (Anderson et al. [38−40]), as shown in Figure 9. The separation in this case is dominated by pressure forces and also by the transport of vorticity causing a vortex lift-off in the intake diffuser. Such separations are termed as vorticity separations and are different from shear driven separations [38]. The flow pathlines of the reversed flow inside the separation bubble, traced on the nacelle surface (Figure 10), clearly shows the presence of a vortex structure, which is very similar to the pathlines of flow in an S-duct having vorticity separations [38,39]. The plot shows a group of circular streamlines which are co-directional (or nearly co-directional), bubble of the intake, a vortical flow field was identified in the intake near the fan_face. Such a vortex structure is beneficial for us, as the presence of the vortex assists in reducing the magnitude of separation and the size of the separation bubble in the intake. In Figure 9, it can be noted that the reversed flow region is much smaller near the plane of symmetry and larger away from the centre of the nacelle. As discussed in the case of VG's, vortices facilitate the transport of energy between the boundary layer and free stream flow and weakens separation. The vortex here exerts a force on the slow moving particles inside the reversed flow region causing them to turn around in the vortex field and get aligned in the direction of free stream, reducing the reversed flow region near the central plane. This is an important feature which becomes significant when considering the effect of blowing as mentioned in the following sections.

4.3. Slot blowing results

For the purposes of this study, we have run simulation cases of 5 different slot types and 3 different levels of blowing pressure ratios. The study has shown that blowing can satisfactorily reduce, and even completely avoid separation in the intake diffuser. But variations in the blowing supply pressure, and also the position, dimension and

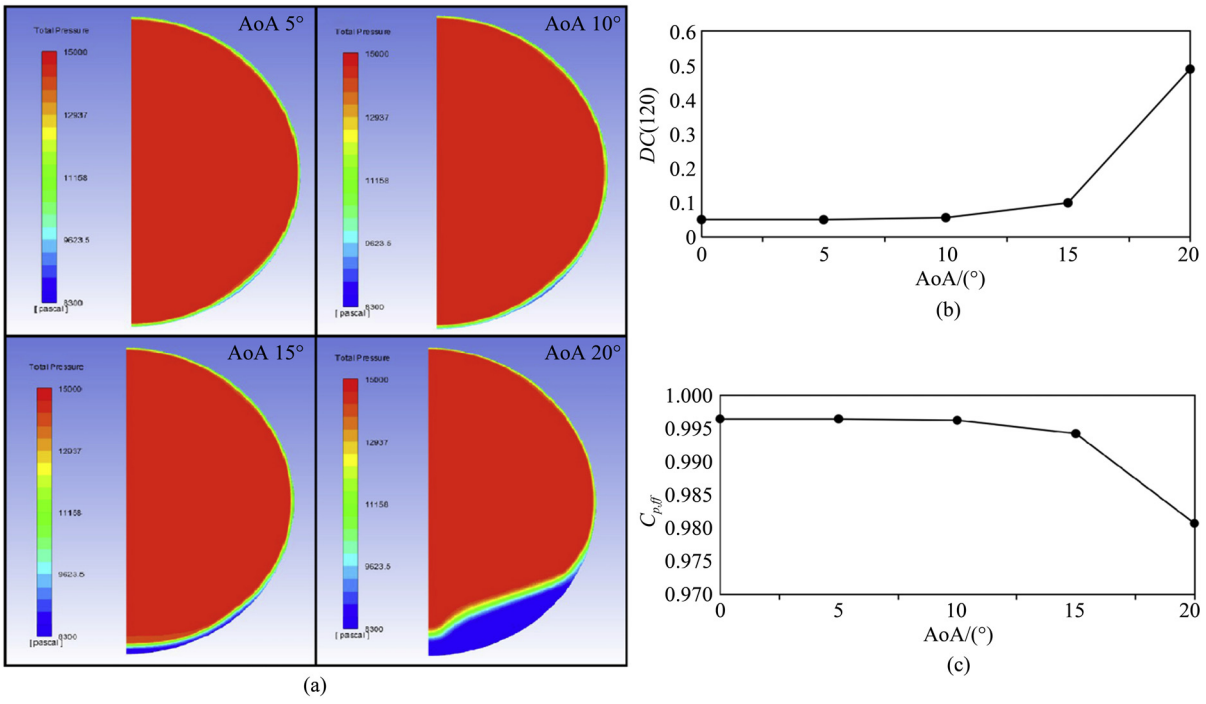

Figure 8 (a) Total pressure (Pa) contours at fan_face, (b) variation of $DC(120)$ distortion descriptor with AoA, (c) variation of $C_{p,ff}$ distortion descriptor with AoA.

orientation of the blowing slot, have strong and noticeable effect on the distortion reduction achieved. We will now discuss and illustrate this with some example cases.

4.3.1. Effect of lip blowing

Let us consider the case of blowing with $PR = 1.1$ at AoA 15°. As discussed before, a very small separation was observed at 15° without any active flow control. The fan-face total pressure contours in Figure 11 show a rise in the pressure recovery within the region where the separated boundary layer was present. Separation has been completely removed at 15° in the intake by all the five slot variations, by applying blowing at a very low blowing pressure ratios of 1.1. One can see from Figure 12(a) that the nacelle drag has also been reduced in all the blowing cases, compared to the baseline case of no blowing.

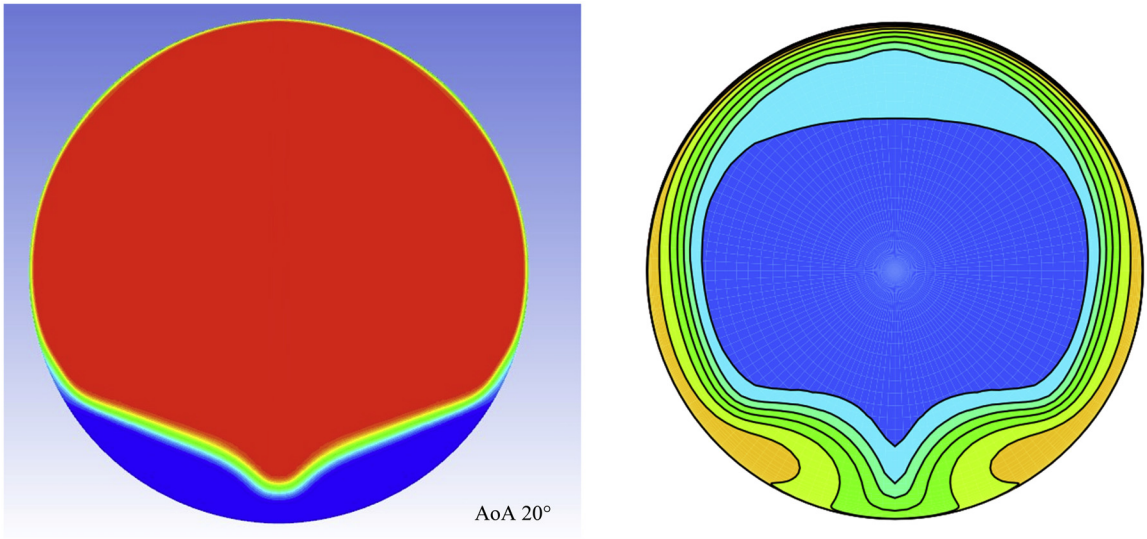

Figure 9 Engine fan-face contours showing distortion in this study (left). Similar contours in S-duct intakes [39] (right).

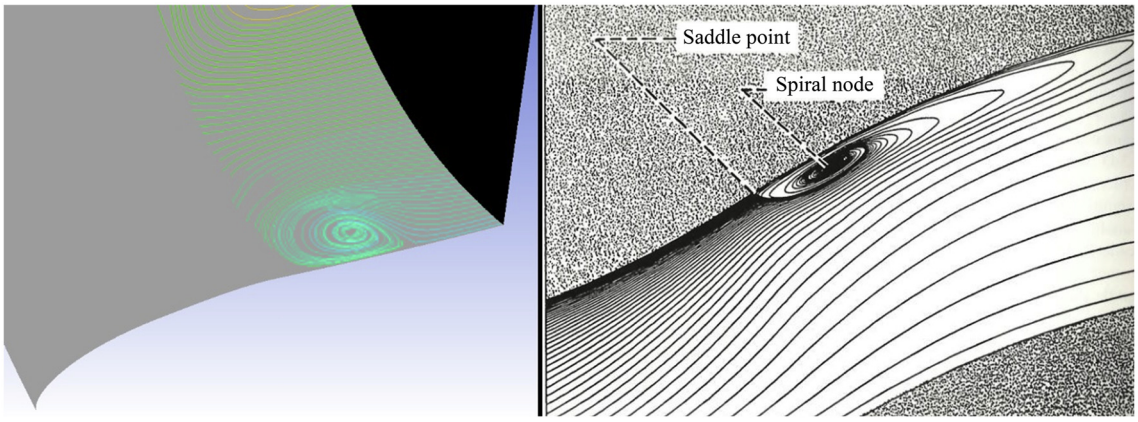

Figure 10 Surface streamlines on the intake diffuser walls in this study (left). Similar streamlines observed in S-duct intakes [38] (right).

Similarly, we can see from the variation in both the fan-face distortion descriptors at 15° AoA, shown in Figure 12(c) and (e), that the level of flow distortion has reduced in all these blowing cases as compared to the baseline no blowing case. Note that the variations in both description descriptors, and also the drag coefficient, for all the slots vary monotonically. Therefore we can say that each slot has a different level of blowing effectiveness, with respect to the reduction in distortion achieved by blowing. The most effective slot in this case is Slot 3, with the lowest modified drag co-efficient C_{D^*}, lowest $DC(120)$ distortion, and highest coefficient of pressure $C_{p,ff}$, (Figure 12(a), (c) and (e) respectively).

The least effective slot at $PR = 1.1$ is Slot 5, although it still outperforms the baseline model in aerodynamic efficiency by removing separation.

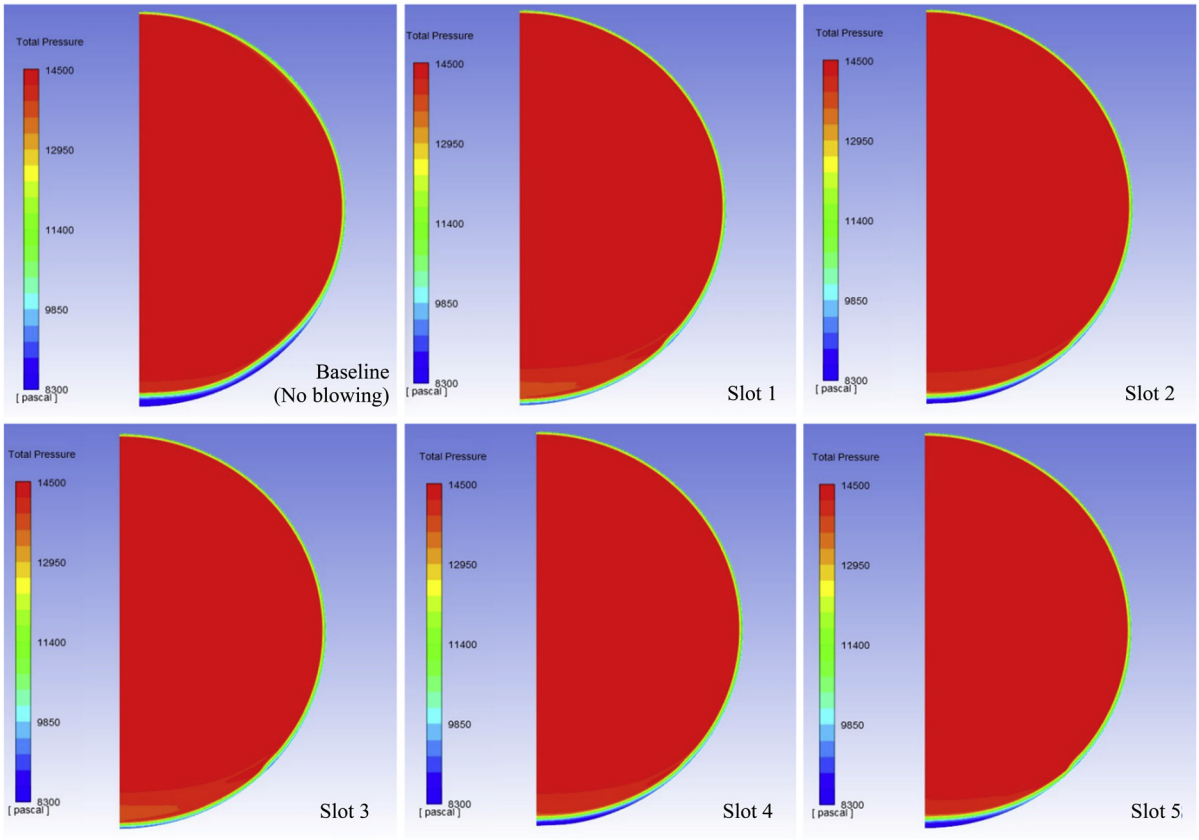

Figure 11 Effect of slot blowing on the fan_face total pressure (Pa) contour at 15° AoA, for different slots at $PR = 1.1$. Separation eliminated with blowing in all cases.

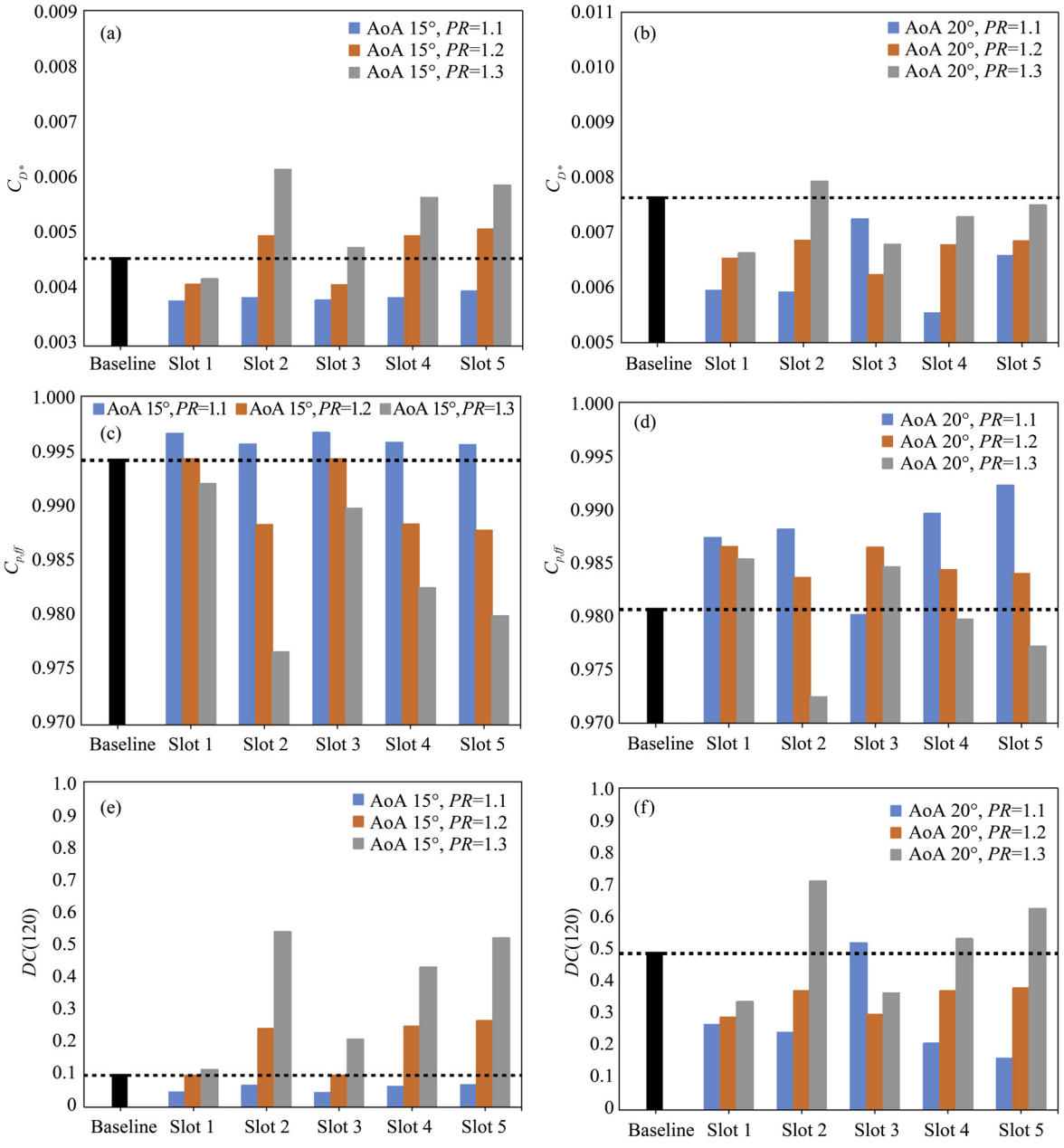

Figure 12 Effect of each slot variant on the modified drag coefficient (C_D*), $DC(120)$ distortion and total pressure coefficient ($C_{p,ff}$), at angle of attack 15° and 20° for different blowing pressure ratios.

4.3.2. *Effect of blowing pressure ratio*

The above conclusion brings up an important point; although blowing can reduce separation and improve efficiency, it can be extremely sensitive with respect to the blowing parameters like the blowing pressure ratio, slot width and angle of blowing, and also the separation conditions in the intake. If the applied pressure ratio is higher than that necessary, it may trigger separation, or worsen a separation which is already present in the intake.

Alternately, if the pressure ratio is lower than that necessary, it would not be sufficient to reduce distortion. Taking Slot 2 at 15° AoA as an example, the distortion falls initially, at a blowing pressure ratio of 1.1, but it increase as the blowing pressure ratio is increased to 1.2 (Figure 12(a), (c) and (e)). This is because the higher pressure ratio increases the blowing mass influx and the velocity of blowing air stream. Since this flow is perpendicular to the free stream, if sufficiently strong, it may initiate separation or strengthen an existing separation.

4.3.3. *Effect of intake vortex structure*

The significance of the interaction between blowing air and the separation vortex, can be seen when comparing the performance of Slot 1 and Slot 2 at a high incidence angle.

At AoA = 15° and *PR* = 1.1, Slot 1 is found to be more effective in reducing distortion as compared to Slot 2, but for the same PR, at AoA = 20°, Slot 2 was found to be more effective. This is because when the separation is stronger, the effects of the vortex structure comes into play, which will require a higher pressure ratio to overcome. A flow feature seen in the case of Slot 3 can be used to understand the nature of this interaction (please refer Figure 13).

It has been mentioned before that the vortex formation in the intake helps in reducing the severity of separation and distortion near the base of the centre plane. If the blowing air is directed at the vortex, it becomes weaker, and this reduces the pressure recovery produced by the intake vortex. At *PR* = 1.1, the benefit from the vortex is reduced while the blowing is not sufficiently strong to overcome separation completely. This is evident from the larger area of reversed flow (Figure 13) at *PR* = 1.1. Weakening of the vortex results in levels of distortion higher than the baseline conditions. In the case of Slot 3, it is clearly visible from the distortion plots (in Figure 14) that blowing at *PR* = 1.1 worsens fan-face distortion but blowing at a *PR* = 1.2 show better performance than baseline. The non-uniformity in the total pressure contours, by which we mean the rise in total pressure recovery near the symmetry plane due to the vortex, is reduced compared to the baseline. By increasing the pressure ratio to 1.3, the vortex is further weakened and there is no longer a sudden increase in pressure recovery near the centre plane, which was present due to the intake vortex. At pressure ratio 1.3, the blowing is more efficient than at *PR* = 1.1 but less efficient than *PR* = 1.2, showing that the efficiency or effectiveness of blowing is highly sensitive to the blowing pressure ratio.

4.3.4. *Effect of slot width and orientation*

The weakening of the vortex and rise in distortion is not present at *PR* = 1.1 in the case of Slot 4 and 5, because these wider slot provide higher mass flow of air than Slot 3 at the same pressure ratio, which is enough to overcome the separation altogether. It was not present in the cases of Slot 1 and Slot 2 because they inject air normal to the free stream flow, causing minimal effect on the vortex. Therefore, in all cases with the exception of Slot 3, the best performance was achieved at a blowing *PR* of 1.1. The tapered duct was found to be more effective than the normal ducts at lower pressure ratios, but as the pressure ratio was increased, performance degraded, and they became less effective than normal duct slots because of high mass injection which triggers separation.

The variations in both distortion descriptors, and also the drag coefficient, for all the slots are synchronous. Each slot has a different level of blowing effectiveness, with respect to the reduction in distortion achieved by blowing.

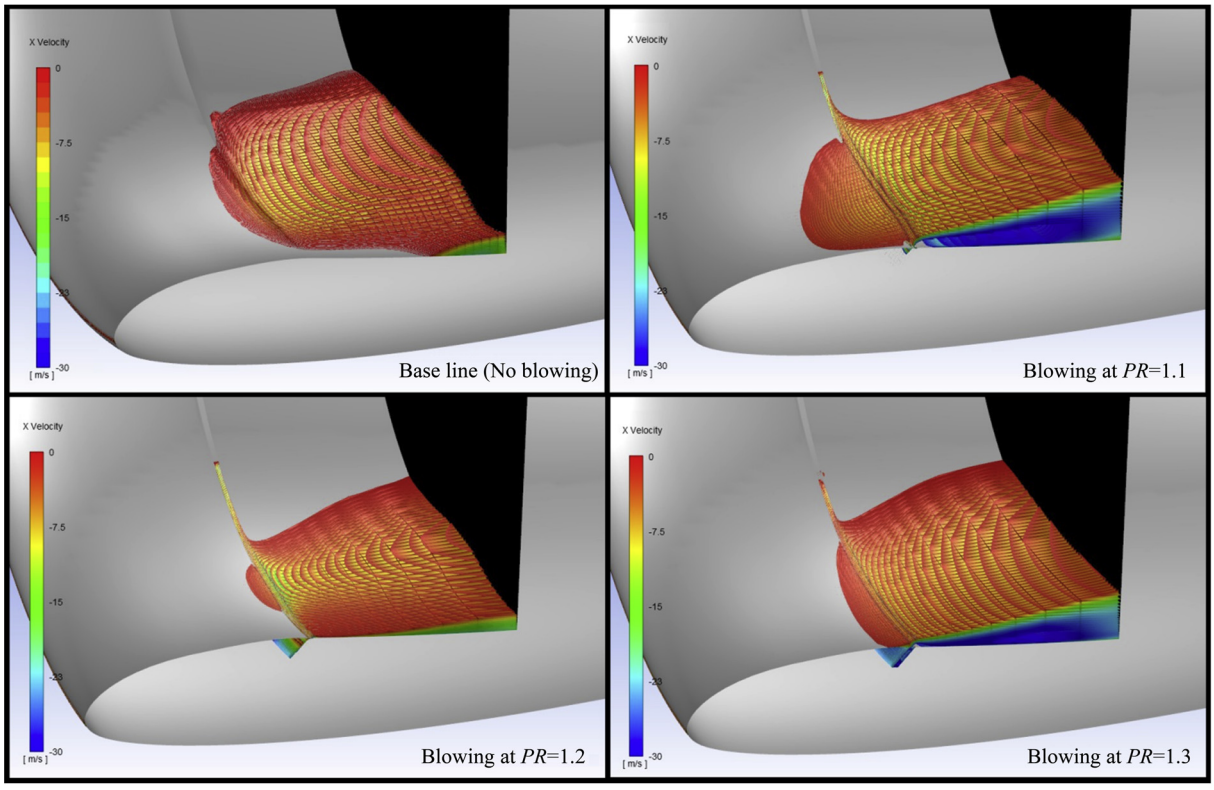

Figure 13 Effect of slot blowing on the intake vortex for strong intake separation at 20° angle of attack. Comparing baseline case and blowing with Slot 3 at different pressure ratios.

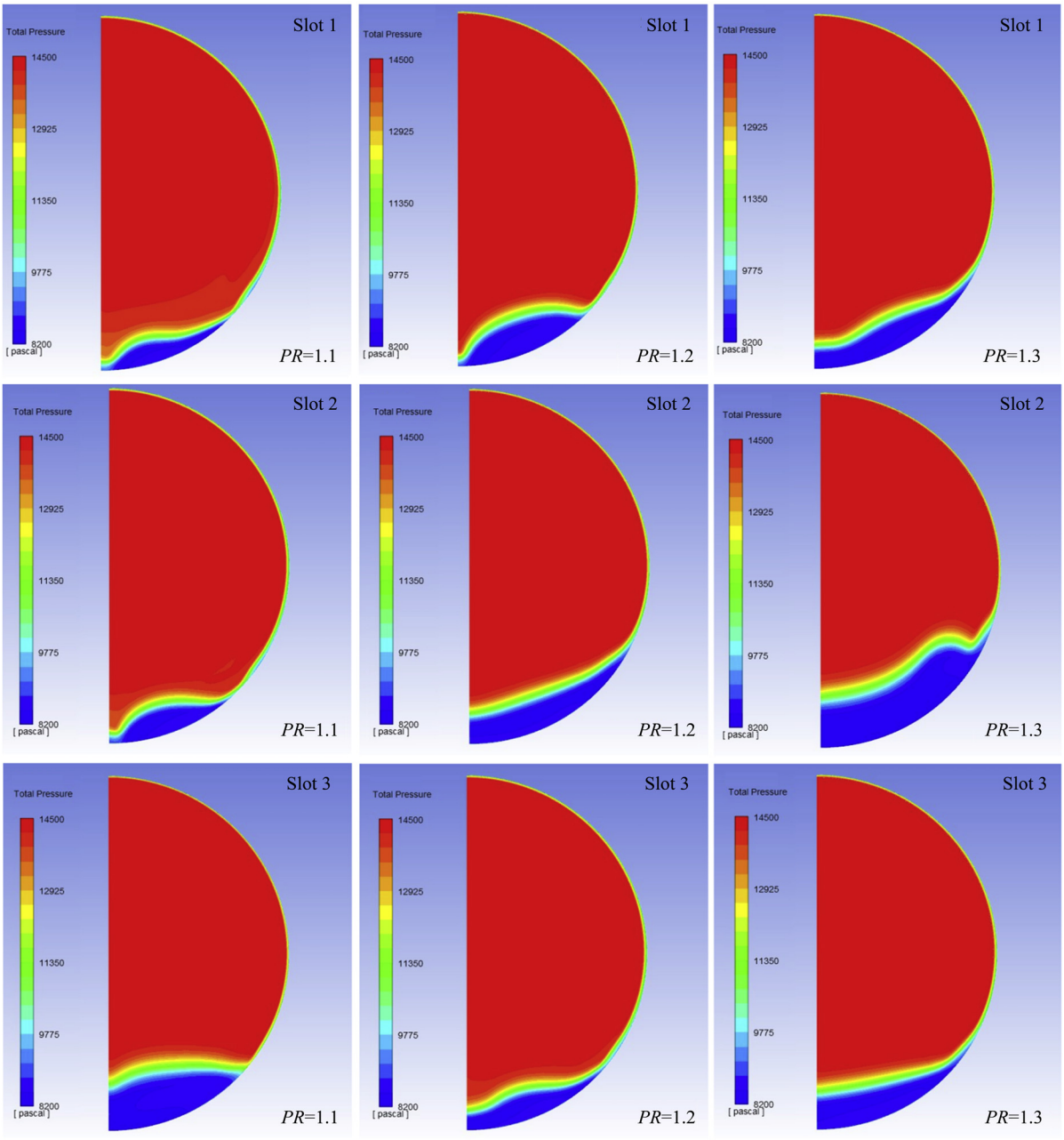

Figure 14 Effect of slot blowing on the fan_face total pressure (Pa) contours, using Slot 1, Slot 2 and Slot 3 with a strong intake separation at 20° angle of attack, at different pressure ratios.

An interesting point to be noted is the pressure contours near the centre plane of the blowing cases from Slot 4 and Slot 5 at low pressure ratios (Figure 15). In these cases the slots are wide enough to provide the mass flow required to remove the vortex structure, but the blowing pressure ratio is not strong enough to fully overcome separation. In these cases, the pressure contoursare similar to those seen in normal serpentine duct intakes and other boundary layer ingesting systems (Cho et al. [41], Wellborn et al. [42]), due to the absence of the vortex lift off.

Another interesting fact to be noted is that the parasitic effect of a separation triggered by blowing increases faster in direct blowing when compared to pitched blowing. That is, when the pressure ratio is changed equally in both the pitched and direct slots, the corresponding changes to the performance is more gradual in the case of the pitched slots than direct slots. This property of skewed slots would provide better control over the blowing and make it easier to tailor it to the specific operating condition. It can also prevent undesirable intake distortion by slowing down the

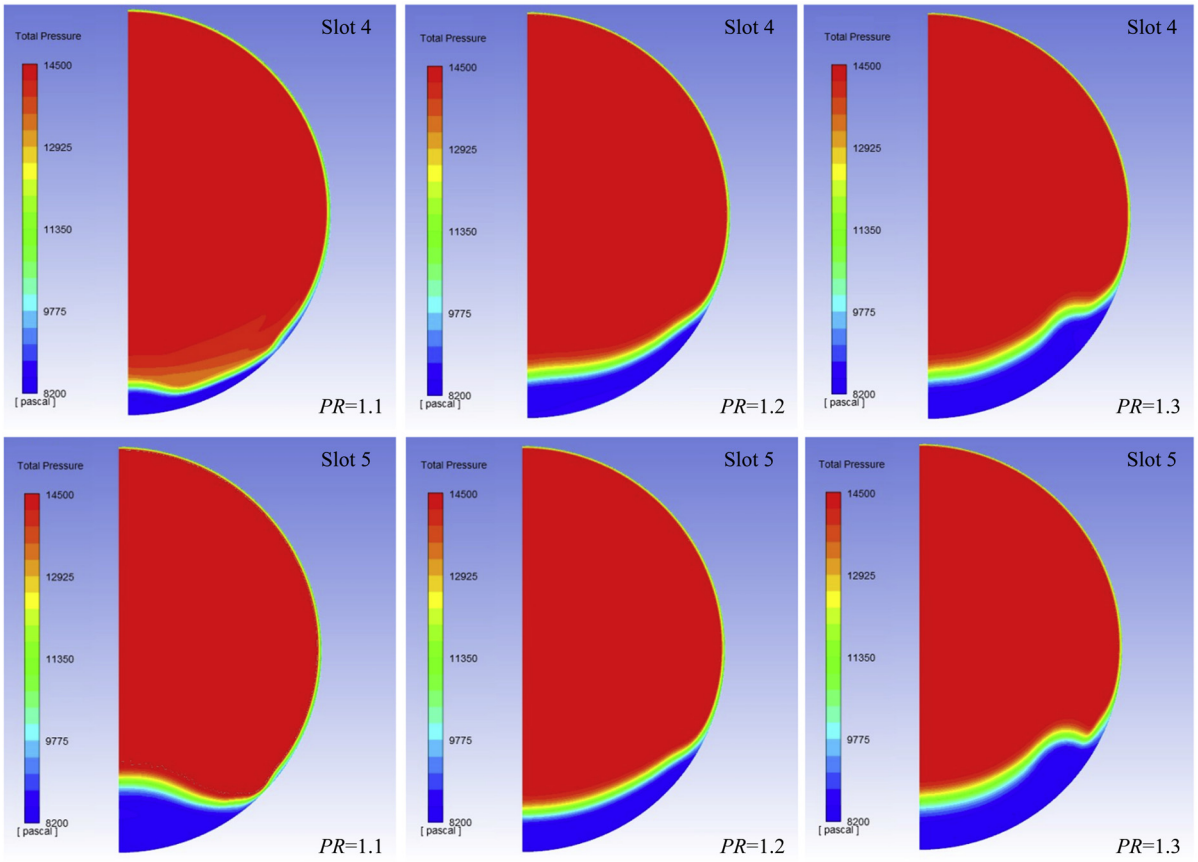

Figure 15 Effect of slot blowing on the fan_face total pressure (Pa) contours, using Slot 4 and Slot 5 with a strong intake separation at 20° angle of attack, at different pressure ratios.

effects like separation growth, if the blowing pressure suddenly changes due to blowing control malfunctions.

5. Conclusions

A CFD based study of the application of active flow control in the intake of a nacelle to reduce fan face distortion has been carried out. Through the angle of attack study, baseline data was obtained, while the intake separation and its features were also studied. Further simulations were carried out to assess the implementation of slot blowing, with five different slot variation being tested to control this separation. Direct and pitched slot blowing were used, and both methods have been shown to effectively reduce intake flow separation and the associated engine face distortion. Separation was completely removed by all the 5 slot variants using a blowing pressure ratio of $PR = 1.1$ at 15° AoA. For the higher AoA cases the separation, and the engine face distortion due to separation, was reduced considerably with slot blowing. The effectiveness of blowing, determined from the reduction in distortion achieved, was found to depend on several factors including flight conditions (like the angle of attack), blowing conditions (blowing pressure ratio, slot dimensions, slot orientation, etc.) and also on the flow and separation conditions inside the intake. No single slot variant was found to be better than all the others in all aspects. The benefit of blowing was different for each slot and was strongly influenced by the different factors mentioned above.

The vortex structure formed in the intake at high angle of attack also strongly influences the effectiveness of blowing. The effectiveness is very sensitive to blowing pressure ratio, both increasing and decreasing with pressure ratio depending on the intake flow conditions, making the blowing pressure ratio a key parameter in separation control.

Slot orientation also has a strong influence on the effectiveness of blowing, as the pitched slots exert a stronger weakening effect on the vortex structure than direct blowing slots. At low blowing pressure ratios and low blowing mass flow, the direct slots were found to reduce distortion more effectively than the pitched slots. At higher pressure ratios, the direct blowing slots may trigger separation, but for the pitched blowing slots, this effect is not as strong as in the direct blowing case. Therefore, at higher pressure ratios, the pitched slots were found to be more effective than the direct slots.

A similar effect was observed with increase in slot dimensions. As the slots were made wider, the blowing mass

flow increases and compensates for the weakening effect on the vortex. Thus better distortion reduction was achieved with pitched blowing in wider slots. Wider and pitched slots were generally found to be more effective than thinner or direct slots respectively. Also the change in the effects caused by blowing at different pressure ratios was more gradual with pitched slots than direct slots. But care must be taken to keep the blowing pressure ration in check so as not to inject too much mass flow into the free stream and triggering separation.

This study establishes proof-of-concept by demonstrating the feasibility of using lip blowing for separation control in aero-intakes via numerical modelling, and therefore further research and experimentation with this method can be undertaken with confidence keeping this study as a starting point or reference. The next step would be to integrate active flow control to slim lip or short intake nacelles, and assess its effectiveness experimentally. Since this study is purely CFD based, conducting wind tunnel tests can validate and confirm the accuracy of results obtained here. Additionally, our research provides crucial insights, regarding the critical design and control parameters (slot dimensions, slot orientation, blowing pressure ratio, etc), that need to be considered while designing such an experiment.

Flow separation generally occurs during unsteady operation, like cross winds, ground vortex intake, very high AoA during take-off or landing, etc, or due to nacelle design constraints like slim-lip or short intakes. This study focused only on high AoA separation at cruise conditions, due to the high computational cost involved with unsteady flow modelling for large domains, and the necessity to retain the NASA CRM geometry for validation purposes. In future work, number of test cases can be expanded to cover the entire flight envelope of an aircraft, while unsteady or transient numerical methods, like the unsteady RANS model, can be applied for flow modelling.

The engine mass flow depends on the engine MFCR, which would strongly affect blowing effectiveness. More test cases in different flight regimes, with varying MFCR, need to be simulated, with different slot widths, more gradual changes in the blowing pressure ratio, different pitching angles of the slot, etc. to determine the best blowing conditions in those flight conditions. As a possible alternative, pulsed blowing (or intermittent blowing) has been shown to reduce the required blowing mass flow without compromising the advantages of continuous blowing (McManus et al. [43,44], Garnier et al. [45]). This technique could be explored to improve the efficiency of blowing.

References

[1] R.W. Luidens, N.O. Stockman, J.H. Diedrich, Optimum Subsonic, High-Angle-Of-Attack Nacelles, SAE Transactions, 1980, pp. 3457−3468.

[2] A. Peters, Z.S. Spakovszky, W.K. Lord, B. Rose, Ultrashort nacelles for low fan pressure ratio propulsors, ASME Journal of Turbomachinery 137 (2) (2015) 021001.1-021001.14.

[3] W.K. Lord, D.G. MacMartin, T.G. Tillman, Flow control opportunities in gas turbine engines, in: Fluids 2000 Conference and Exhibit, 2000, AIAA 2000-2234.

[4] C. Freeman, A.L. Rowe, Intake engine interactions of a modern large turbofan engine, in: ASME 1999 International Gas Turbine and Aeroengine Congress and Exhibition, 1999, Paper No: 99-GT-344.

[5] J. Flatt, The history of boundary layer control research in the United States of America, in: G.V. Lachmann (Ed.), Boundary Layer and Flow Control, 1961, pp. 122−143.

[6] M. Gad-el-Hak, Flow Control: Passive, Active, and Reactive Flow Management, Cambridge University Press, Cambridge, 2000.

[7] D.G. MacMynowski, D.R. Williams, Flow control terminology, in: Fundamentals and Applications of Modern Flow Control, American Institute of Aeronautics and Astronautics, 2008, pp. 59−71.

[8] M. Gad-el-Hak, Modern developments in flow control, Appl. Mech. Rev. 49 (1996) 365−379.

[9] M. Gad-el-Hak, Introduction to flow control, in: Flow Control: Fundamentals and Practices, Springer-Verlag, 1998, pp. 1−108.

[10] J.C. Lin, F.G. Howard, V.G. Shelby, Small submerged vortex generators for turbulent flow separation control, J. Spacecraft Rockets 27 (5) (1990) 503−507.

[11] G.B. Schubauer, W.G. Spangenberg, Forced mixing in boundary layers, J. Fluid Mech. 8 (1) (1960) 10−32.

[12] G.E.A. Meier, Prandtl's boundary layer concept and the work in Göttingen, in: Proceedings of the IUTAM Symposium on One Hundred Years of Boundary Layer Research, DLR-Göttingen, Germany, August 12−14, 2004.

[13] R.A. Wallis, The Use of Air Jets for Boundary-Layer Control, A.R.L., Australia, Aero, Note 110, 1952.

[14] J.P. Johnston, M. Nishi, Vortex generator jets - means for flow separation control, AIAA J. 28 (6) (1990) 989−994.

[15] S.D. Erbslöh, W.J. Crowther, Control of Boundary Layer Separation on a Civil Turbofan Intake Using Air-Jet Vortex Generators, CEAS KATnet Conference on Key Aerodynamic Technologies, Bremen, 2015.

[16] V. Kumar, F.S. Alvi, Use of high-speed microjets for active separation control in diffusers, AIAA J. 44 (2) (2006) 273−281.

[17] V. Kumar, Separation Control in Adverse Pressure Gradients Using High-Speed Microjets, PhD. Dissertation, FAMU-FSU College of Engineering, Florida State University, United States, 2008.

[18] M. Amitay, Synthetic jets and their applications for fluid/thermal systems, in: J.F. Morrison, D.M. Birch, P. Lavoie (Eds.), IUTAM Symposium on Flow Control and MEMS, 2008.

[19] M. Amitay, D. Pitt, A. Glezer, Separation control in duct flows, J. Aircraft 39 (4) (2002) 616−620.

[20] D. McCormick, Boundary layer separation control with directed synthetic jets, in: 38th Aerospace Sciences Meeting and Exhibit, 2000, AIAA-2000-0519.

[21] V. Tesar, C.H. Hung, W.B. Zimmerman, No-moving-part hybrid-synthetic jet actuator, Sensor Actuator Phys. 125 (2) (2005) 159−169.

[22] T. Kühn, V. Ciobaca, R. Rudnik, B. Gölling, W. Breitenstein, Active flow separation control on a high-lift wing-body configuration, part 1: baseline flow and constant blowing, in: 29th AIAA Applied Aerodynamics Conference, Honolulu, Hawaii, 2011, AIAA 2011-3168.

[23] V. Ciobaca, T. Kühn, R. Rudnik, M. Bauer, B. Gölling, Active flow separation control on a high-lift wing-body configuration, part 2: the pulsed blowing application, in: 29th AIAA Applied Aerodynamics Conference, Honolulu, Hawaii, 2011, AIAA 2011-3169.

[24] A.L. Johns, R.C. Williams, H.C. Potonides, Performance of a V/STOL tilt nacelle inlet with blowing boundary layer control, in: 15th Joint Propulsion Conference, 1979, AIAA-79-1163.

[25] Ministry Industry Drag Analysis Panel Study Group, Guide to In-Fight Thrust Measurement of Turbojets and Fan Engines, AGARD, 2008, AGARD-AG-237.

[26] J.C. Vassberg, M.A. DeHaan, S.M. Rivers, R.A. Wahls, Development of a common research model for applied CFD validation studies, in:

26th AIAA Applied Aerodynamics Conference, 2008, AIAA-2008-6919.
[27] J. Seddon, E.L. Goldsmith, Intake Aerodynamics, Second ed., Blackwell Science, Oxford, 1999.
[28] D.W. Levy, T. Zickuhr, J.C. Vassberg, S. Agarwal, R.A. Wahls, S. Pirzadeh, M.J. Hemsch, Summary of Data from the First AIAA CFD Drag Prediction Workshop, 2002, AIAA 2002-0841.
[29] J. Vassberg, E. Tinoco, M. Mani, B. Rider, T. Zickuhr, D. Levy, O. Brodersen, B. Eisfeld, S. Crippa, R. Wahls, J. Morrison, D. Mavriplis, M. Murayama, Summary of the fourth AIAA CFD drag prediction workshop, in: 28th AIAA Applied Aerodynamics Conference, 2010, AIAA 2010-4547.
[30] M. Rivers, NASA Common Research Model, URL: https://commonresearchmodel.larc.nasa.gov/ [Accessed: 10-3-2022].
[31] T.P. Stańkowski, D.G. MacManus, C.T. Sheaf, N. Grech, Aerodynamic interference for aero-engine installations, in: 54th AIAA Aerospace Sciences Meeting, San Diego, California, USA, 2016.
[32] T.P. Stańkowski, D.G. MacManus, C.T. Sheaf, R. Christie, Aerodynamics of aero-engine installation, Proc. IME G J. Aero. Eng. 230 (14) (2016) 2673−2692.
[33] I.B. Celik, U. Ghia, P.J. Roache, C.J. Freitas, H. Coleman, P. Raad, Procedure for estimation and reporting of uncertainty due to discretization in CFD applications, J. Fluid Eng. 130 (7) (2008) 078001.
[34] P.J. Roache, Verification and Validation in Computational Science and Engineering, Hermosa Publishers, Albuquerque, New Mexico, 1998.
[35] J.W. Slater, Examining Spatial (Grid) Convergence, URL: https://www.grc.nasa.gov/www/wind/valid/tutorial/spatconv.html, [Accessed: 10-03-2022].
[36] E.N. Tinoco, O.P. Brodersen, S. Keye, K.R. Laflin, E. Feltrop, J.C. Vassberg, M. Murayama, Summary data from the sixth AIAA CFD drag prediction workshop: CRM cases, J. Aircraft 55 (4) (2018) 1352−1379.
[37] M. Rivers, EXPERIMENT RESULTS SEARCH, https://commonresearchmodel.larc.nasa.gov/experiment-results-search/ [Accessed: 10-3-2022].
[38] B.H. Anderson, C.E. Towne, Application of computational fluid dynamics to inlets, in: J. Seddon, J.E.L. Goldsmith (Eds.), Practical Intake Aerodynamic Design, Second ed., Blackwell Science, Oxford, 1994.
[39] B.H. Anderson, H.D. Baust, J. Agrell, Management of Total Pressure Recovery, Distortion and High Cycle Fatigue in Compact Air Vehicle Inlets, 2002, NASA TM-2002-212000.
[40] B.H. Anderson, J. Gibb, Application of computational fluid dynamics to the study of vortex flow control for the management of inlet distortion, in: 28th Joint Propulsion Conference and Exhibit, 1992, AIAA 92-3177.
[41] S.Y. Cho, I. Greber, Three-dimensional Compressible Turbulent Computations for a Non-diffusing S-Duct, Lewis Research Center, 1994, NASA-CR-4391.
[42] S.R. Wellborn, B.A. Reichert, T.H. Okiishi, An experimental investigation of the flow in a diffusing S-duct, in: 28th Joint Propulsion Conference and Exhibit, 1992, AIAA-1992-3622.
[43] K. McManus, H.H. Legner, S.J. Davis, Pulsed vortex generator jets for active control of flow separation, in: Fluid Dynamics Conference, 1994, AIAA-1994-2218.
[44] K. McManus, J. Magill, Airfoil performance enhancement using pulsed jet separation control, in: 4th Shear Flow Control Conference, 1997, AIAA-1997-1971.
[45] E. Garnier, M. Leplat, J.C. Monnier, J. Delva, Flow Control by Pulsed Jet in a Highly Bended S-Duct, 6th AIAA Flow Control Conference, 2012, AIAA-2012-3250.

Nacelle intake flow separation reduction at cruise conditions using active flow control

Nambiar, Vinayak Ramachandran

2022-10-17

Nambiar VR, Pachidis V. (2022) Nacelle intake flow separation reduction at cruise conditions using active flow control, Propulsion and Power Research, Volume 11, Issue 3, September 2022, pp. 337-352

https://doi.org/10.1016/j.jppr.2022.07.005